Optimal noise suppression in Fresnel incoherent correlation holography (FINCH) configured for maximum imaging resolution

Barak Katz,* Dov Wulich, and Joseph Rosen

Department of Electrical and Computer Engineering, Ben Gurion University of the Negev, P.O. Box 653, Beer-Sheva 84105, Israel

*Corresponding author: barakk@ee.bgu.ac.il

Received 12 July 2010; accepted 3 September 2010;
posted 13 September 2010 (Doc. ID 131543); published 14 October 2010

An optimal setup in the sense of imaging resolution for the Fresnel incoherent correlation holography (FINCH) system is proposed and analyzed. Experimental results of the proposed setup in reflection mode suffer from low signal-to-noise ratio (SNR) due to a granular noise. SNR improvement is achieved by two methods that rely on increasing the initial amount of phase-shifted recorded holograms. In the first method, we average over several independent complex-valued digital holograms obtained by recording different sets of three digital phase-shifted holograms. In the second method, the least-squares solution for solving a system of an overdetermined set of linear equations is approximated by utilizing the Moore–Penrose pseudoinverse. These methods improve the resolution of the reconstructed image due to their ability to reveal fine and weak details of the observed object.

OCIS codes: 090.1995, 030.6140, 110.4280.

1. Introduction

Fresnel incoherent correlation holography (FINCH) is a relatively new method of digital holography for recording holograms under incoherent illumination [1–4]. FINCH is a single-channel nonscanning holographic system in which spatially incoherent light is reflected or emitted from a three-dimensional (3D) object, then propagates through a spatial light modulator (SLM), and is finally recorded by a digital camera as a raw digital hologram. The SLM is used as a diffractive beam splitter of the incoherent interferometer so that each spherical beam, originating from each object point, is split into two spherical beams with two different curve radii. Accumulation of the entire interference within all of the couples of spherical beams creates the Fresnel hologram of the observed object.

FINCH has been demonstrated by our group for several scenarios: digital holograms of white-light reflecting objects [1] and fluorescent objects [2], fluorescence holographic microscopy [3], and, most recently, a FINCH-based synthetic aperture system [4]. However, the FINCH has not been analyzed yet in order to find an optimal configuration in any sense. In this study, we analyze the system and propose an optimal setup in the sense of maximal imaging resolution.

Our analysis in the next section starts with the general, yet simple configuration of FINCH—the lensless FINCH [4]. From the general case, we choose the configuration that is optimal in the sense of imaging resolution. However, we show that due to practical constraints, the optimal configuration can only be realized by a FINCH equipped with a refractive lens. This later configuration was actually used in the experiments of Refs. [1–3], as well as in most of the experiments of the present study.

Another problem that we deal in this paper is the specklelike noise adjoined to the reconstructed images. The noise seems unavoidable in the process of creating the complex-valued hologram (CVH) by

0003-6935/10/305757-07$15.00/0

the phase-shifting procedure [1–4]. Every CVH is a linear superposition of three recorded holograms, each of which is recorded where the SLM mask is displayed with a different phase constant. This process of capturing three holograms is necessary in order to remove the twin image and the bias term from the captured hologram. The specklelike noise originates from the shot noise of the digital camera, and since the holographic signal is of the order of the noise, the latter severely affects the quality of the best in-focus reconstructed image. Two different approaches to suppress the noise are presented in this study, and both rely on increasing the initial amount of phase-shifted recorded holograms. In the first approach, the noise suppression is inspired from many other techniques of averaging over several independent speckle images [5]. In the second approach, we approximate a solution for an overdetermined set of linear equations using the Moore–Penrose pseudoinverse. With this type of system, there are more constraining equations than there are free variables, and, therefore, it is impossible to find a single solution that satisfies all linear equations of the system. Yet, the least-squares solution can be approximated using the Moore–Penrose pseudoinverse [6]. In contrast to other noise reduction methods [7–16], these proposed noise suppression methods are motionless and do not make use of any postprocessing operations, such as filtering of the reconstructed images. The optimal setup and the noise suppression techniques are discussed in the following sections.

2. Optimal Configuration of FINCH

The goal of the following analysis is to find the optimal configuration of FINCH in the sense of maximum imaging resolution. In order to achieve this goal, we calculate the point spread function (PSF) of the recording stage of the FINCH shown in Fig. 1(a).

As mentioned above, the SLM is used as a diffractive beam splitter of the incoherent interferometer so that each spherical beam originating from each object point is split into two spherical beams with two different curve radii. The beam splitting is achieved by displaying on the SLM a combination of two diffractive lenses, expressed by the sum $Q[-1/f_1]+Q[-1/f_2]$, where the quadratic phase function is designated by the function Q, such that $Q[a]=\exp[i\pi a\lambda^{-1}(x^2+y^2)]$. f_1 and f_2 are the focal lengths of the two diffractive lenses, where we assume, without loss of generality, that both diffractive lenses are positive. In order to simplify our notation, we consider the imaging only from one specific transverse plane, the plane that is located a distance f_1 before the SLM. It can be assumed that the transverse resolution of the image at any other nearby planes has similar properties. For an arbitrary object point in a distance f_1 before the SLM, at $(\bar{r}_s,0)$, where $\bar{r}_s=(x_s,y_s)$, the complex amplitude on the SLM plane in the paraxial approximation is given by the expression [17] $C_1(\bar{r}_s)L[-\bar{r}_s/f_1]Q[1/f_1]$, where the linear phase function is designated by the function L, such

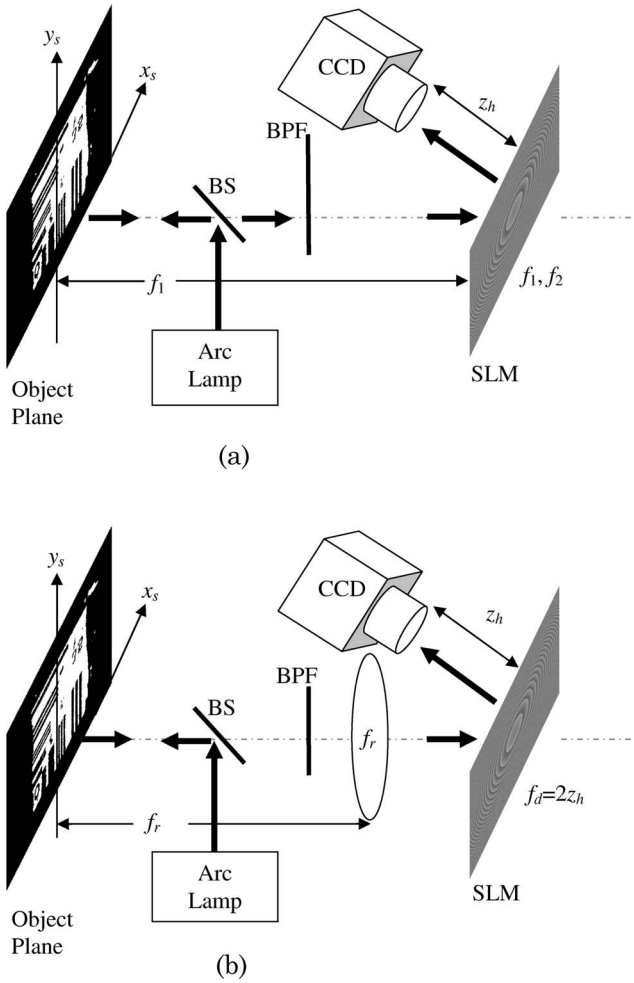

Fig. 1. Possible experimental setups: (a) Lensless FINCH, (b) FINCH with a positive refractive lens. BS—beam splitter. BPF—bandpass filter. CCD—charge-coupled device. SLM—spatial light modulator.

that $L[\bar{b}]=\exp[i2\pi\lambda^{-1}(b_x x+b_y y)]$, and $C_1(\bar{r}_s)$ is a $\bar{r}_s$ dependent complex constant. The PSF of the recording stage of FINCH is the intensity on the plane $\bar{r}_o=(x_o,y_o)$, recorded by the digital camera, located a distance z_h beyond the SLM, as the result of the illuminating object point at $(\bar{r}_s,0)$. This PSF is given by

$$
\begin{aligned}
I_h(\bar{r}_o;\bar{r}_s) &= \left|\left\{C_1(\bar{r}_s)L\left[\frac{-\bar{r}_s}{f_1}\right]Q\left[\frac{1}{f_1}\right]\right.\right.\\
&\quad\left.\left.\times\left(Q\left[\frac{-1}{f_1}\right]+Q\left[\frac{-1}{f_2}\right]\right)\right\}*Q\left[\frac{1}{z_h}\right]\right|^2\\
&= \left(C_2+C_3(\bar{r}_s)Q\left[\frac{-1}{z_r}\right]L\left[\frac{-\bar{r}_r}{z_r}\right]\right.\\
&\quad\left.+C_3^*(\bar{r}_s)Q\left[\frac{1}{z_r}\right]L\left[\frac{\bar{r}_r}{z_r}\right]\right),
\end{aligned}
\tag{1}
$$

where the asterisk in the second line denotes a two-dimensional convolution, and $C_{2,3}$ are complex constants. The first two lines of Eq. (1) describe

the process of recording FINCH of a point source in which the tilted spherical wave hits the SLM with its two diffractive lenses, then split to two different spherical waves that propagate a distance z_h to the digital camera, where the squared absolute of the wave interference is recorded. The parameters of the second part of Eq. (1) derived from the first part are

$$z_r = \pm(f_e + z_h), \quad \text{where} \quad f_e = f_1 f_2/(f_2 - f_1) \tag{2}$$

and

$$\bar{r}_r = \bar{r}_s z_h/f_1, \quad \text{where } \bar{r}_r = (x_r, y_r). \tag{3}$$

The second part of Eq. (1) is the typical expression of an in-line Fresnel hologram of a single point. To avoid the problem of the twin image, the second (or the third) term in the second part of Eq. (1) should be isolated by the phase-shifting procedure. Reconstructing this term by the Fresnel back propagation yields the image of the point at a distance z_r from the hologram given by Eq. (2), and at a transverse location $\bar{r}_r = (x_r, y_r)$ given by Eq. (3). The sign "±" in Eq. (2) indicates the possibility to reconstruct from the hologram either the virtual or the real image, according to which term, second or third, is chosen from the second part of Eq. (1). Based on Eq. (3), the transverse magnification of this FINCH is

$$M_T = \partial \bar{r}_r/\partial \bar{r}_s = z_h/f_1. \tag{4}$$

Unlike conventional imaging systems, in general, the transverse magnification of FINCH does not satisfy the relation $M_T = z_r/z_i$, where z_i is the distance from the object to the input aperture, or to the SLM in the FINCH case. Consequently, even if the input and the output apertures of FINCH are equal, FINCH does not satisfy the relation $M_T = \mathrm{NA_{in}}/\mathrm{NA_{out}}$, where $\mathrm{NA_{in}}$ and $\mathrm{NA_{out}}$ are the numerical apertures of the input and output apertures, respectively. Therefore, in FINCH, the loss of the image resolution might happen either by limited input or by limited output numerical apertures. In other words, assuming the system is diffraction limited, the minimal resolved object size observed by the FINCH is given by

$$\begin{aligned}\Delta_{\min} &= \max\{\lambda/\mathrm{NA_{in}}, \lambda/(M_T \mathrm{NA_{out}})\} \\ &= \max\{2\lambda f_1/D_{\mathrm{SLM}}, 2\lambda|z_r|/(M_T D_{\mathrm{CCD}})\},\end{aligned} \tag{5}$$

where D_{SLM} and D_{CCD} are the diameters of the SLM and the digital camera, respectively. For a given $\mathrm{NA_{in}}$, it is undesired to lose a resolution due to the output aperture. Therefore, referring to Eq. (5), an optimal FINCH satisfies the inequality

$$2\lambda f_1/D_{\mathrm{SLM}} \geq 2\lambda|z_r|/(M_T D_{\mathrm{CCD}}). \tag{6}$$

Assuming the diameters of the SLM and the digital camera are equal, substituting Eqs. (2) and (4) into Eq. (6) yields the condition on the value of f_e as follows:

$$-2z_h \leq f_e < 0. \tag{7}$$

Practically, the fill factor of the SLM is less than 100%, and therefore the constant phase modulation inherently exists in the SLM. Consequently, choosing two focal lengths, f_1 and $f_2 < \infty$, could cause three, instead of two, unwanted waves mixing on the hologram plane—one wave due to the constant phase and another two due to the two different diffractive lenses. This practical limitation can be solved without any resolution reduction by introducing a refractive lens with focal lens f_r in front of the SLM, as is shown in Fig. 1(b). In this case, a constant phase together with a single positive diffractive lens with focal lens f_d are displayed on the SLM, thus splitting the incoming wave to exactly two waves. Assuming the object point is located a distance f_r before the refractive lens, at $(\bar{r}_s, 0)$, the new PSF is given by

$$\begin{aligned}I_h(\bar{r}_o; \bar{r}_s) &= \left| \left\{ C_1(\bar{r}_s) L\left[\frac{-\bar{r}_s}{f_r}\right] Q\left[\frac{1}{f_r}\right] Q\left[\frac{-1}{f_r}\right] \right.\right. \\ &\quad \left.\left. \times \left(1 + Q\left[\frac{-1}{f_d}\right]\right) \right\} * Q\left[\frac{1}{z_h}\right] \right|^2 \\ &= \left(C_2 + C_3(\bar{r}_s) Q\left[\frac{-1}{z_r}\right] L\left[\frac{-\bar{r}_r}{z_r}\right] \right. \\ &\quad \left. + C_3^*(\bar{r}_s) Q\left[\frac{1}{z_r}\right] L\left[\frac{\bar{r}_r}{z_r}\right] \right),\end{aligned} \tag{8}$$

where calculating the second part of Eq. (8) indicates that $z_r = \pm(z_h - f_d)$, and $\bar{r}_r = \bar{r}_s z_h/f_r$. Following the reasoning of Eqs. (5) and (6) and noting that the relation $f_e = -f_d$ exists in the modified FINCH with the refractive lens, the condition in which the system remains limited by the input aperture is

$$f_{\min} \leq f_d \leq 2z_h, \tag{9}$$

where $f_{\min}$ is the minimal focal distance of the diffractive lens that can be displayed on the SLM. However, a focal distance smaller than $2z_h$ reduces the fringe visibility of the hologram, and hence, setting focal distance at $f_d = 2z_h$ becomes the optimal value.

Equation (8) is the expression of the transparency function of a hologram created by an object point and recorded by a conventional FINCH [1–3], and consequently $I_h(\bar{r}_o; \bar{r}_s)$ is the PSF of the recording system. The complete Fresnel hologram of a general incoherently illuminated object $I_s(x_s, y_s, z_s)$ is an integral of the PSF given by Eq. (8) over all the object intensity distribution as follows:

$$H(x_o, y_o) = \iiint I_s(x_s, y_s, z_s) I_h(x_o, y_o; x_s, y_s, z_s) \mathrm{d}x_s \mathrm{d}y_s \mathrm{d}z_s. \tag{10}$$

To conclude this section, optimal setup in the sense of resolution is attained once the focal distance of the positive diffractive lens on the SLM is twice the distance between the SLM and the digital camera, and the wavefront originating from an object point arrives on the SLM as a plane wave. The last condition indicates that the distance between the refractive lens and the SLM does not have any influence on the resolution of the system.

3. Noise Suppression Techniques

In this section, we deal with the noise accompanying the reconstructed images. As mentioned earlier, the main source of the noise in all our experiments is the shot noise of the digital camera. In the case of low-contrast reflective objects, the problem of low SNR becomes severe so that some technique of noise suppression must be involved in order to observe the image with an acceptable quality. The noise is granular in its nature and looks like speckle noise, although it is by no means related to the speckle noise associated with coherent holography. In order to suppress the noise, we should refer back to the phase-shifting method of on-axis holography.

The twin image and the bias terms of a recorded hologram in an on-axis setup can be eliminated by recording three holograms, each of which is recorded with a different phase constant α_j of the SLM mask, obtaining a set of linear equations in three free variables of the form $H_N = A_{N\times 3}X_3$, $N = 3$, as follows:

$$\left.\begin{aligned} H_1(x,y;t_1) &= B + H_f\exp(i\alpha_1) + H_f^*\exp(-i\alpha_1)\\ H_2(x,y;t_2) &= B + H_f\exp(i\alpha_2) + H_f^*\exp(-i\alpha_2)\\ H_3(x,y;t_3) &= B + H_f\exp(i\alpha_3) + H_f^*\exp(-i\alpha_3) \end{aligned}\right\}, \tag{11}$$

where $H = \{H_1(x,y;t_1), H_2(x,y;t_2), H_3(x,y;t_3)\}^T$ is the vector of the raw holograms set recorded by the digital camera at times t_1, t_2, and t_3, respectively; $A = \{\{1, \exp(i\alpha_1), \exp(-i\alpha_1)\}; \{1, \exp(i\alpha_2), \exp(-i\alpha_2)\}; \{1, \exp(i\alpha_3), \exp(-i\alpha_3)\}\}$ is the matrix of the phase-shifting constants; $X = \{B, H_f, H_f^*\}^T$ is the vector of free variables; and the asterisk denotes the conjugate sign. H_f, which is the CVH without the useless bias B and the twin image H_f^* terms, is obtained by solving the above set of linear equations, where the solution is the well-known equation of the three holograms superposition [1,2], given by

$$\begin{aligned} H_f(x,y) = {} & H_1(x,y;t_1)[\exp(-i\alpha_3) - \exp(-i\alpha_2)]\\ & + H_2(x,y;t_2)[\exp(-i\alpha_1) - \exp(-i\alpha_3)]\\ & + H_3(x,y;t_3)[\exp(-i\alpha_2) - \exp(-i\alpha_1)]. \end{aligned} \tag{12}$$

Stepwise phase shift differences of $2\pi/3$ are used so that a complete phase cycle of 2π is accomplished.

Speckle noise can be modeled as the random walk problem in the complex domain, assuming the phase of the noise signals is equally likely to lie anywhere in the primary interval $(-\pi, \pi)$ [5]. In this case, we assume that the specklelike noise $n(x,y;t)$ is additive and the obtained CVH is given by $\hat{H}_f(x,y;t) = H_f(x,y;t) + n(x,y;t)$. Increasing the number of recorded holograms set to $N = 3M$ in a stepwise phase shift of $2\pi/N$ permits M independent CVHs. Each CVH, $\hat{H}_f(x,y;t)$, is generated by a different subset of three different recorded holograms, subsets that preserve the stepwise phase shift differences of $2\pi/3$. Each independent CVH contains the same object hologram $H_f(x,y;t)$, yet it also contains a superimposed random specklelike noise $n(x,y;t)$. According to the first approach proposed in this study, noise suppression is achieved by averaging over the available independent CVHs as follows: $\bar{H}_M(x,y) = \frac{1}{M}\sum_{i=1}^{M}\hat{H}_f(x,y;t_i)$. It is a well-known result [5] that, for an independent random noise, the standard deviation of the averaged random variable is related to $1/\sqrt{M}$. Therefore, the SNR of the reconstructed image from a hologram averaged over M independent CVHs is expected to increase with $\sqrt{M}$.

The second approach utilizes the optimal solution attained by the Moore–Penrose pseudoinverse for the noise suppression purpose. Increasing the number of recorded holograms in the initial set to $N > 3$ yields a system of an overdetermined set of linear equations in three variables of the form $H_N = A_{N\times 3}X_3$, $N > 3$, in which there are more constrained equations than free variables in the system. In this situation, a single general solution that satisfies all available equations does not exist. However, by utilizing the Moore–Penrose pseudoinverse, a least-squares solution of the form $X_3 = \tilde{A}_{N\times 3}H_N$ that minimizes the norm $\|H_N - A_{N\times 3}X_3\|$ can be found, where the pseudoinverse matrix is calculated as follows:

$$\tilde{A} = (A^TA)^{-1}A^T. \tag{13}$$

$A = \{\{1, \exp(i\alpha_1), \exp(-i\alpha_1)\}; \ldots; \{1, \exp(i\alpha_N), \exp(-i\alpha_N)\}\}$. The vector of free variables terms $X = \{B, H_f, H_f^*\}^T$, which includes the desired noise-suppressed hologram $\tilde{H}_f$, is obtained by $X_3 = \tilde{A}_{N\times 3}H_N$, where $H = \{H_1(x,y;t_1), H_2(x,y;t_2), \ldots, H_N(x,y;t_N)\}^T$ is the vector of the raw holograms set recorded by the digital camera at times $t_1, t_2, \ldots, t_N$, respectively.

4. Experimental Results

Three different experiments have been conducted to assess the proposed methods. In the first experiment, the proposed noise suppression method has been validated. Once the SNR has been improved, the optimal resolution setup could have been evaluated in the second experiment, whereas in the last experiment, a comprehensive test of the optimal configuration is demonstrated. The experiments have been conducted according to the setup shown in Fig. 1(b). A resolution target, 3 mm × 3 mm in size, containing both vertical and horizontal binary gratings with line density ranging from 4.3 to 8.5 lines per mm, has been tested in the experiments. The focal distances of the refractive and diffractive lenses have been 50 and 68 cm,

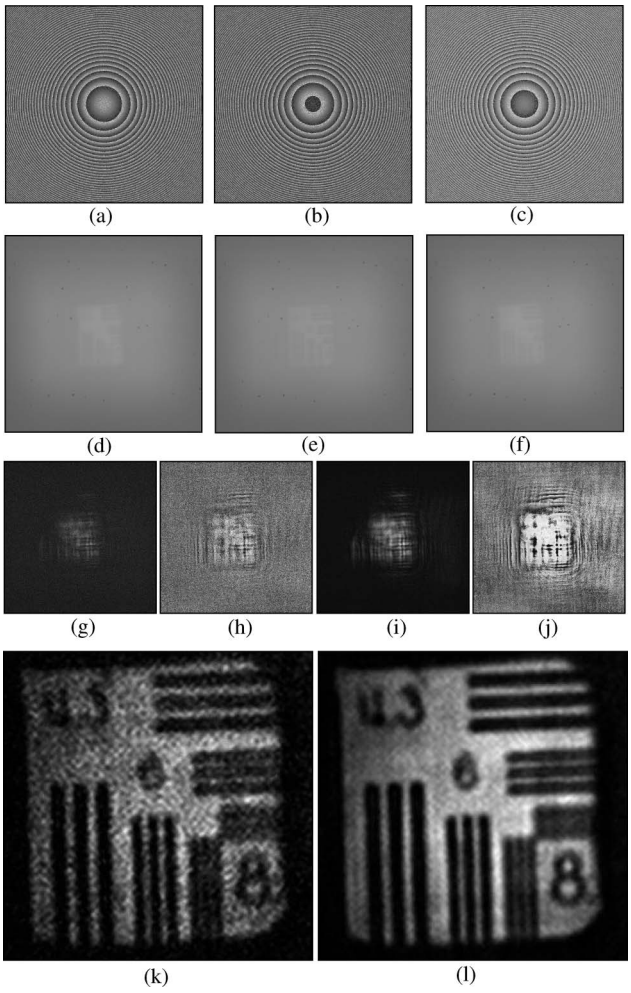

Fig. 2. Results of the proposed noise suppression method. (a)–(c) are the three masks displayed on the SLM during the recording process of the raw holograms presented in (d)–(f), (g)–(h) are the magnitude and phase of the noisy CVH generated from three raw holograms, and (i) and (j) are the noise-suppressed CVH generated from 36 raw holograms. (k) and (l) are the corresponding best in-focus reconstructed planes from the holograms (g), (h) and (i), (j), respectively.

respectively, and the target has been located at the back focal plane of the refractive lens. The distance z_h between the phase-only SLM (HOLOEYE, PLUTO) and the CCD (PixelFly) has been 34 cm. A 100 W halogen arc lamp has been used for the object illumination, and a bandpass filter (BPF) with a 40 nm bandwidth surrounding a 550 nm central wavelength has been placed just in front of the refractive lens. Since the SLM is a phase-only modulator, each diffractive phase element is distributed randomly among half of the SLM pixels [1–4]. Each raw hologram has been recorded with an optimal exposure time, i.e., the longest exposure time before reaching the point of camera saturation, and the entire recorded holograms superposed, according to Eq. (12). The results of the first experiment are summarized in Figs. 2 and 3, the results of the second experiment are summarized in Fig. 4, and the results of the last experiment are summarized in Fig. 5. In the first experiment, $M = 12$ different CVHs have been generated based on the 36 recorded holograms. Figures 2(a)–2(c) present three masks, out of 36, displayed on the SLM during the holograms recording process. The three masks in Figs. 2(a)–2(c) have three phase factors: 0°, 120°, and 240°, respectively. The three raw holograms obtained by displaying on the SLM the three masks of Figs. 2(a)–2(c) are shown in Figs. 2(d)–2(f), respectively.

Figures 2(g)–2(j) present the magnitude and the phase of the CVH generated from only three raw holograms, and of an averaged CVH generated by averaging over $M = 12$ CVHs, respectively. The best in-focus reconstructed plane, computed by Fresnel back propagation, corresponding to the two holograms presented in Figs. 2(g) and 2(j), are depicted in Figs. 2(k) and 2(l). It can be seen that the resolution along the horizontal and vertical directions of the reconstructed image is improved in Fig. 2(l) in the sense that this image reveals some of the original high-frequency gratings. A quantitative comparison of

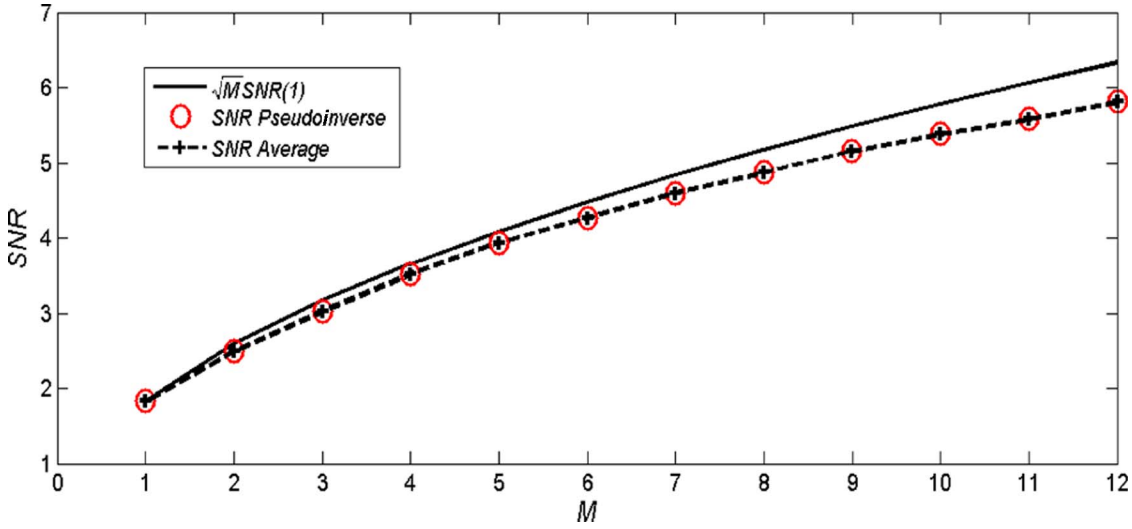

Fig. 3. (Color online) Comparative results of the SNR obtained by the averaging approach and by the pseudoinverse approach versus the theoretical graph $\sqrt{M}\mathrm{SNR}(1)$.

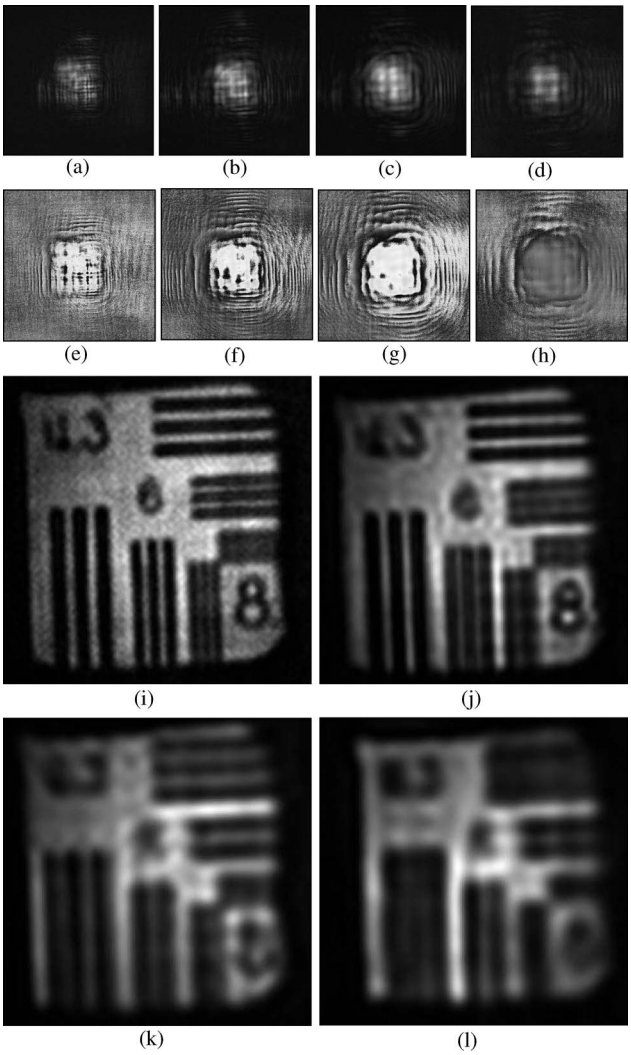

Fig. 4. Evaluation of the optimal resolution setup. The magnitude of noise-suppressed holograms is shown with (a) $f_d = 2z_h$, (b) $f_d = 3z_h$, (c) $f_d = 4z_h$, and (d) lensless FINCH. The phase of noise-suppressed holograms is shown with (e) $f_d = 2z_h$, (f) $f_d = 3z_h$, (g) $f_d = 4z_h$, and (h) lensless FINCH. The best in-focus reconstructed plane from the noise-suppressed holograms is shown with (i) $f_d = 2z_h$, (j) $f_d = 3z_h$, (k) $f_d = 4z_h$, and (l) lensless FINCH.

the various holograms is carried out by measuring the SNR in different typical, relatively uniform areas from the best in-focus reconstructed image, versus M, ranging from 1 to 12 average CVHs. The SNR is defined as $\mathrm{SNR} = \frac{|\mu|}{\sigma} = |\frac{1}{KL}\sum_{k=1}^{K}\sum_{l=1}^{L}P(k,l)|/\sqrt{\frac{1}{KL}\sum_{k=1}^{K}\sum_{l=1}^{L}|P(k,l)-\frac{1}{KL}\sum_{k=1}^{K}\sum_{l=1}^{L}P(k,l)|^2}$, where μ and σ are the mean and standard deviation of the specklelike noise on an uniform intensity $P(k,l)$ on the best in-focus reconstructed plane; k, l are the coordinates of each pixel; and K, L are the dimensions of the considered area. Apparently, an improved quality of the reconstructed images is achieved by increasing the number of holograms in the recorded hologram set. It can be shown that the standard deviation σ_M of the average over the sum of M independent random variables satisfies the relation $\sigma_M = \sigma_1/\sqrt{M}$. Thus, Fig. 3 shows a comparison between the theoretical curve of SNR ($= \mathrm{SNR}(1)\cdot\sqrt{M}$) and the experimental SNR for different averages of CVHs ranging from $M = 1$ to $M = 12$, as well as for the pseudoinverse hologram. The results indicate that in the case of our on-axis setup, the best in-focus reconstructed plane obtained by averaging M independent CVH is identical to the result obtained by the pseudoinverse method, and that both methods are optimal in the sense of noise suppression. The difference between the experimental and theoretical curves of Fig. 3 can be explained by some weak statistical dependence between the noise samples, whereas the theoretical curve is based on a pure independence.

In the second experiment, the noise-suppressed hologram is generated by the optimal setup with a recorded set of 36 hologram. The magnitude and the phase of this hologram are shown in Figs. 4(a) and 4(e), respectively. This optimal hologram has been compared with three other noise-suppressed holograms recorded by suboptimal setups; in the first and second modified configurations, the focal distance of the diffractive lens displayed on the SLMs has been changed from the optimal focal distance of $2z_h (z_h = 34\ \mathrm{cm})$ to focal distances of $3z_h$ and $4z_h$, respectively. In the third modified configuration, the refractive lens has been removed (making it a lensless FINCH), and the object has been brought

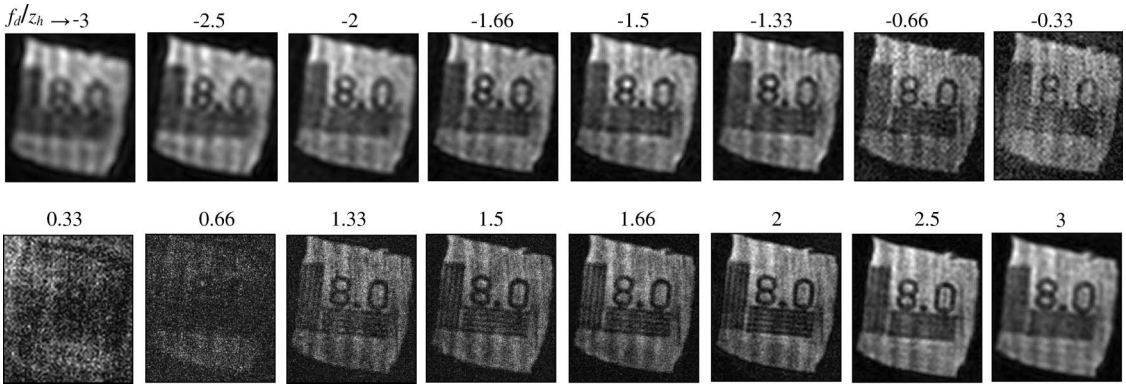

Fig. 5. Set of the best in-focus reconstructed planes from holograms recorded with diffractive lenses ranging between $f_d = -3z_h$ to $3z_h$.

closer to the SLM for preserving the input numerical aperture. In addition, the phase element displayed on the SLM has been chosen to be a diffractive lens with the shortest focal distance that can be achieved with the SLM having a pixel size of 8 μm. The shortest focal distance guarantees maximum resolution power for a given aperture size. In the case of the PLUTO SLM aperture (1080×1080 pixels), where each diffractive phase element is distributed randomly among half of the SLM pixels, the minimal focal distance has been 23 cm. All four noise-suppressed holograms have been generated from a recorded set of 36 holograms and an input numerical aperture that equals to 0.0086. The magnitude of the noise-suppressed holograms recorded with the optimal setup, as well as with the first, second, and third suboptimal noise-suppressed holograms, are shown in Figs. 4(a)–4(d), respectively. The phases of these holograms are depicted in Figs. 4(e)–4(h), respectively. The best in-focus reconstructed plane of the noise-suppressed hologram recorded with the optimal setup, as well as those of the first, second, and third modified configurations, are presented in Figs. 4(i)–4(l), respectively. As expected, the best resolved image has been obtained for the noise-suppressed hologram recorded by the optimal setup, as is demonstrated in Fig. 4(i), in comparison to Figs. 4(j)–4(l). It can be seen that Fig. 4(i) is indeed superior in the sense of resolution in comparison to all other best in-focus reconstructed planes, and that the resolution is consistently deteriorated with increasing the focal distance beyond the optimal focal length of $f_d = 2z_h$.

A comprehensive test of the optimal configuration is demonstrated in the third experiment and presented in Fig. 5. The best in-focus reconstructions from holograms captured with diffractive lenses ranging from $f_d = -3z_h$ to $3z_h$ are shown in the figure. The resolution target used in this part contains both vertical and horizontal binary gratings with line density of 8 lines per mm. These results confirm that the optimal focal length for the diffractive lens is indeed $f_d = 2z_h$.

5. Conclusions

In this paper, we have pointed out the optimal setup of FINCH in the sense of maximum imaging resolution. For FINCH equipped with a refractive lens, the conclusion in this aspect is that the maximum resolution is obtained when the focal lens of the positive diffractive lens is equal to twice the distance between the SLM and the digital camera.

We have also demonstrated two methods of noise suppression for a FINCH system. Both methods rely on increasing the amount of phase-shifted recorded holograms, and both have been completely equivalent. The proposed methods are motionless, and they might be effective for coherent digital holography, as well.

References

1. J. Rosen and G. Brooker, "Digital spatially incoherent Fresnel holography," Opt. Lett. **32**, 912–914 (2007).
2. J. Rosen and G. Brooker, "Fluorescence incoherent color holography," Opt. Express **15**, 2244–2250 (2007).
3. J. Rosen and G. Brooker, "Non-scanning motionless fluorescence three-dimensional holographic microscopy," Nat. Photon. **2**, 190–195 (2008).
4. B. Katz and J. Rosen, "Super-resolution in incoherent optical imaging using synthetic aperture with Fresnel elements," Opt. Express **18**, 962–972 (2010).
5. J. W. Goodman, "Statistical properties of laser speckle patterns," in *Laser Speckle and Related Phenomena*, J. C. Dainty, ed., Vol. 9 of Topics in Applied Physics (Springer–Verlag, 1975), pp. 9–75.
6. P. Lancaster and M. Tismenetsky, *The Theory of Matrices*, 2nd ed. (Academic, 1985), pp. 432–438.
7. J. P. Huignard, J. P. Herriau, L. Pichon, and A. Marrakchi, "Speckle-free imaging in four-wave mixing experiments with $Bi_{12}SiO_{20}$ crystals," Opt. Lett. **5**, 436–437 (1980).
8. F. Wyrowski and O. Bryngdahl, "Speckle-free reconstruction in digital holography," J. Opt. Soc. Am. A **6**, 1171–1174 (1989).
9. A. Capanni, L. Pezzati, D. Bertani, M. Cetica, and F. Francini, "Phase-shifting speckle interferometry: a noise reduction filter for phase unwrapping," Opt. Eng. **36**, 2466–2472 (1997).
10. A. Brozeit, J. Burke, H. Helmers, H. Sagehorn, and R. Schuh, "Noise reduction in electronic speckle pattern interferometry fringes by merging orthogonally polarized speckle fields," Opt. Laser Technol. **30**, 325–329 (1998).
11. S.-H. Shin and B. Javidi, "Speckle-reduced three-dimensional volume holographic display by use of integral imaging," Appl. Opt. **41**, 2644–2649 (2002).
12. J. Kauffmann, M. Gahr, and H. J. Tiziani, "Noise reduction in speckle pattern interferometry," Proc. SPIE **4933**, 9–14 (2003).
13. Y. Morimoto, T. Nomura, M. Fujigaki, S. Yoneyama, and I. Takahashi, "Deformation measurement by phase-shifting digital holography," Exp. Mech. **45**, 65–70 (2005).
14. T. Nomura, M. Okamura, E. Nitanai, and T. Numata, "Speckles removal in digital holography using multiple wavelengths/distances from an object," in *LEOS 2006. 19th Annual Meeting of the IEEE* (Lasers and Electro-Optics Society, 2006), pp. 74–75..
15. T. Baumbach, E. Kolenovic, V. Kebbel, and W. Jüptner, "Improvement of accuracy in digital holography by use of multiple holograms," Appl. Opt. **45**, 6077–6085 (2006).
16. L. Rong, W. Xiao, and F. Pan, "Reduction of speckle noise in digital holography by multiple holograms," Proc. SPIE **7382**, 73823T (2009).
17. J. W. Goodman, *Introduction to Fourier Optics*, 2nd ed. (McGraw–Hill, 1996), pp. 314–317.